LA-UR -81-1712

Los Alamos National Laboratory is operated by the University of California for the United States Department of Energy under contract W-7405-ENG-36

TITLE PHOTOEMISSION MEASUREMENTS FOR LOW-ENERGY X-RAY-DETECTOR APPLICATIONS

AUTHOR(S) Robert H. Day, P-14

SUBMITTED TO Low Energy X-Ray Conference
Monterey, California
June 1981

photoemission Measurements for Low Energy X-Ray Detector Applications

Robert H. Day

Los Alamos National Laboratory, P. O. Box 1663, MS-410, Los Alamos, NM 87545

ABSTRACT

Photoemission has been studied for nearly 100 years as both a means of investigating quantum physics, and as a practical technique for transducing optical/x-ray photons into electrical currents. Numerous x-ray detection schemes, such as streak cameras and x-ray sensitive diodes, exploit this process because of its simplicity, adaptability, and speed. Recent emphasis on diagnostics for low temperature, high density, and short-lived, plasmas for inertial confinement fusion has stimulated interest in x-ray photoemission in the sub-kilovolt regime. In this paper, a review of x-ray photoemission measurements in the 50 eV to 10 keV x-ray region is given and the experimental techniques are reviewed. A semiempirical model of x-ray photoemission is discussed and compared to experimental measurements. Finally, examples of absolutely calibrated instruments are shown.

INTRODUCTION

The subject of this afternoon's session will focus our attention on detectors for sub-keV x-ray plasma diagnostics. It is frequently desirable to transform x-ray emission into an electrical current for subsequent recording and the photoelectric effect is a useful mechanism for transducing electromagnetic radiation into free electrons. This paper is a brief review of this process as it applies to pulsed plasma x-ray detectors.

The photoelectric process is conceptually simple as outlined schematically in Fig. 1. Radiation incident on a photosensitive surface interacts with the cathode via photoelectric absorption or Compton scattering, creating energetic primary and Auger electrons. These electrons traverse the material creating low energy secondary electrons. Some fraction of the primary and secondary electrons are emitted from the surface of the photocathode.

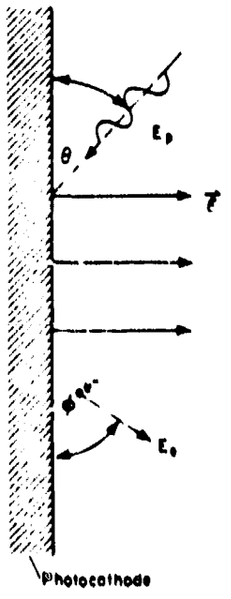

Fig. 1. Schematic of the photoelectron emission process.

This emission is a complicated function of space, energy, and time characterized by the distribution $N(E_e, E_p, \Theta, \phi, t)$, where E_e is the emitted electron energy, Ep is the incident photon energy, Θ is the photon angle of incidence from the photocathode surface, ϕ is the electron emission angle relative to the photocathode surface, and t is time. Photoelectrons are extracted by an applied electric field, $\vec{E}$, and can be used directly as the detector signal or the photocathode return current can be measured.

The photoelectric process has three important properties which make it useful in low energy x-ray pulsed plasma detectors.

1. Speed: The intrinsic speed of the photoelectric emission is $<10^{-17}$s. Transport of electrons to the surface takes $<10^{-14}$s and collection of the emitted current can take $<10^{-12}$ s.
2. Linearity: For many metallic photocathodes and modest extraction field, the process is linear to better than 1% over 15 orders of magnitude in photon intensity.
3. Simplicity: The technique is adaptable to many experimental geometries, is sensitive over a broad range of x-ray energies, and can be tailored to specific needs by choice of materials.

Because of these features, photoelectric emission has found widespread use in many detector systems. This paper reviews the status of our knowledge of this process as it applies to the design, calibration, and use of low energy x-ray diagnostics. It starts with an historical perspective on research into this process and then summarizes a model of photoemission. The measuring techniques of each major differential electron distribution are described and typical experimental data is presented. The long term stability of the photoelectric emission process is discussed and it is shown how these elements are applied in a practical, absolutely calibrated, sub-keV x-ray spectrometer system.

HISTORICAL PERSPECTIVE

Photoelectric emission is one thread in the fabric of modern physics which is deeply woven into the tapestry of quantum electrodynamics. The photoelectric effect has been observed, studied, and utilized for nearly 100 years with the first descriptions reported in 1887 by Hertz,(1) Schuster,(2) and Arrhenius.(3)

During the next 18 years, the basic properties of photoemission were discovered:

1. The total emitted current is linear with electromagnetic intensity.
2. The highest electron energy increases linearly with the exciting photon's energy irrespective of the incident intensity.
3. The emission is essentially instantaneous.

It was recognized that properties 2 and 3 in the list above are incompatible with Maxwell's classical electromagnetic theory and this contradiction motivated the second of Albert Einstein's three seminal papers published in Annalen der Physik in 1905.(4) It was entitled "On a Heuristic Viewpoint Concerning the Production and Transformation of Light" and laid the groundwork for representing photons as localized

particles with energy and momentum. During the next 20 years, detailed experimental investigations by Millikan(5), Compton(6), and others established the photon as the particle component of the electromagnetic wave-particle duality.

As interest in the photoelectric effect fell behind the frontiers of quantum physics, interest increased in applying this unique process to a broad range of applications. Many modern detector systems such as ionization chambers, proportional counters, photomultiplier tubes, photodiodes, x-ray streak and framing cameras make use of this effect.

PHOTOEMISSION MODELS

Despite nearly 100 years of research, we still do not have a complete theory of photoelectric emission as it applies to practical detector systems. The mechanisms that must be accurately modeled include: 1) the generation of the primary electron either through photoelectric absorption or incoherent scattering, 2) the transport of primary and Auger electrons to the photocathode surface and their energy loss to secondaries, and 3) the generation of a detectable signal from these electrons. Of these three steps, the secondary generation and transport process is by far the least well-understood.

The photon interaction is dominated by photoelectric absorption and recent theoretical studies by Pratt, et al.(7) demonstrate that good models of photoelectric cross sections exist above ten kilovolts. More important, for a predictive model of detector behavior, excellent compilations of x-ray cross sections are available for all elements at photon energies above 100 eV,(8-11) and for selected elements at lower energies.(12-13) Thus, it is possible to model the primary electron production mechanism quite accurately.

The primary electron transport and secondary generation and transport provides a much greater challenge. A typical electron distribution, dN/dE_e, for photoemitted electrons is shown in Fig. 2 as reprinted from Henke, et al.(14) The important features of this spectrum are "no loss" peaks for the photo and Auger electrons, their associated loss tails, and a large secondary electron emission in a distribution a few eV wide below 10 eV.

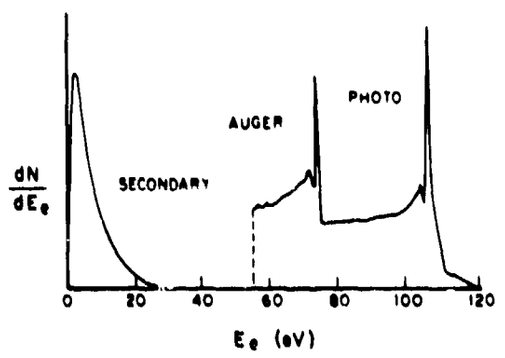

Fig. 2. A typical photoemission spectrum.

Henke, et al.(14) have proposed a semiempirical model that accounts for the "no loss" peak and provides shapes of the secondary electron distribution. The model has also been modified to account for the internal electron scattering processes in semiconductors and insulators.(15) Though absolute predictions of electron yield or spectra, are not yet possible, this model quite accurately predicts the shape of the secondary electron distribution and the photon energy dependence of the total emitted electron yield.

Once an accurate model or measurement of the electron distribution at the surface of the photocathode has been obtained, the transport of this distribution through the electron-optical detector is usually well understood. This step establishes the time response of the detector system. For example, the energy width of the secondary electron distribution establishes the maximum time resolution in a streak camera system.

Similarly, the rise time, t_r, of a photodiode detector is given by the flight-time of the electrons across an anode-cathode gap spacing, d,(16). For an anode-cathode gap voltage, V, $t_r \propto d/\sqrt{V}$. This functional dependence has been verified(17) and the data is shown in Fig. 3. With modest accelerating voltages, ~3 kV, and anode-cathode gap spacings of the order of 1-mm, it is possible to build photodiode detector systems with sub-100 ps response times.

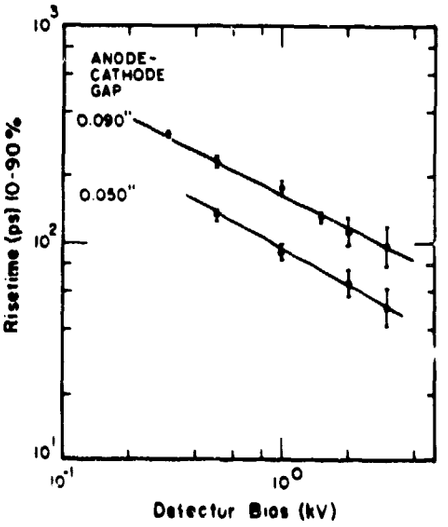

Fig. 3. Detector risetime versus anode-cathode gap voltage and anode-cathode separation.

PHOTOEMISSION DATA

Because there is no complete theory of photoemission, and photoemission is a surface phenomenon which depends critically on surface condition and contaminants, it is necessary to perform extensive measurements on individual materials and geometries of practical interest. Each parameter in the electron distribution, E_p, E_e, C, and e, critically affects different types of detector systems.

In the following subsections, a brief description will be given of how a particular parameter affects different types of diagnostic devices, the techniques utilized to measure the parameter. Samples of the available data will be presented with comparison to models when possible.

No attempt is made to compile a complete bibliography of the available data in the text of this paper. Rather, it is presented in the Appendix as a thorough but not exhaustive list of references on photoemission data above 10 eV. Tables are also included which organize the different types of data by element and energy.

A. Quantum Efficiency dN/dE_p

The quantum efficiency, number of electrons emitted per incident photon, is the most common photoemission data and is required for most absolutely calibrated systems.

A quantum efficiency experiment is performed as shown schematically in Fig. 4. A monochromatic photon beam is incident on the photocathode, and the incident flux and emitted current are monitored to derive the quantum efficiency. The primary beam energy is changed and the photon energy dependence is determined.

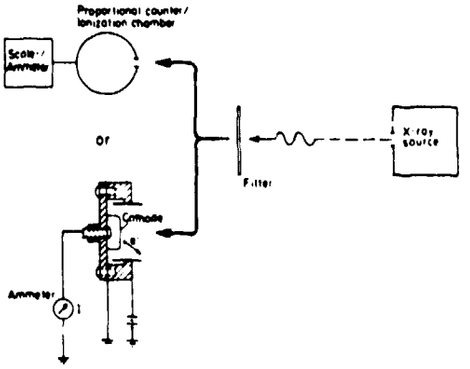

Fig. 4. Quantum efficiency measurements are performed by comparing the emitted photoelectron current to the x-ray flux.

Many such measurements have been made on a wide variety of metallic, semiconductor, and insulating surfaces as part of detector development programs over the past 50 years. Our interest in characterizing x-ray detectors for subkilovolt x-ray measurements has required extending this data into the 50 eV to 1 keV photon energy regime where few measurements have been made. Typical results for photon energies of 20 eV to 10 keV are shown in Fig. 5 for photocathodes of gold, aluminum, copper, and nickel. Many references for this type of data are listed in Table I of the Appendix.

The best available photoemission models such as Henke's model mentioned above, predict quantum efficiencies, QE, with an energy dependence:

$$QE \propto F_p \cdot \mu(E_p)^{-1} \cdot f(E_p)$$

where $\mu(E_p)$ is the incident radiation photoelectric cross section and $f(E_p)$ is a slowly varying function of photon energy related to the efficiency of converting photo and Auger electrons into secondaries.

To test this result, $QE/(\mu(E) \cdot E)$ vs E is plotted in Fig. 6 for carbon, aluminum, and gold samples. The resultant curve is the energy dependence of f(E). The lines drawn through the data points of Fig. 6 are provided to guide the eye and do not represent a model of f(E).

In general, f(E) is a slowly varying function of energy and the $\mu(E) \cdot E$ term accounts for most of the two or three orders of magnitude variation in quantum efficiency. For gold, f(E) does not vary by more than 20-30% from 20 eV to 10 keV. A small anomaly is seen near 150 eV at the N absorption feature and again at 1.8 keV at the M absorption edge. Aluminum shows the largest absorption edge and large changes in f(E) over the entire range of energies. The aluminum surface was modeled as Al_2O_3, and if we use a pure aluminum surface, the effect is even more pronounced. For the carbon surface, f(E) is again slowly varying except at very low energies and with a 30% decrease from 100 eV to 1.5 keV.

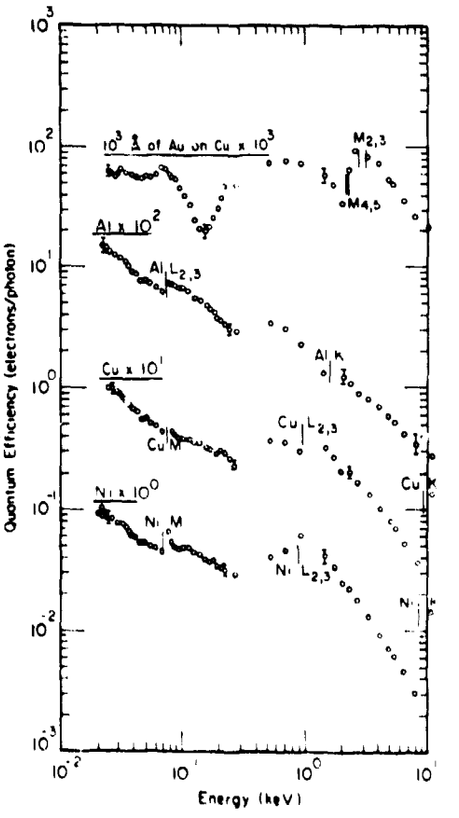

Fig. 5. Quantum efficiencies for gold, aluminum, copper, and nickel. Quantum efficiency is defined as the number of electrons emitted per incident photon.

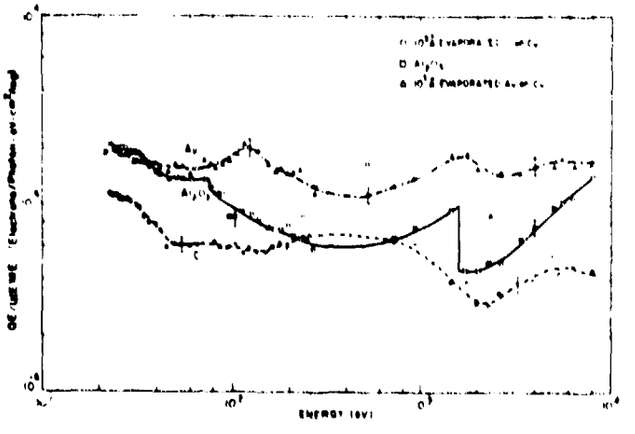

Fig. 6. Energy dependence of f(E) for carbon, Al_2O_3, and gold.

B. Electron Spectra, dN/dE_e

As indicated above, the electron spectrum is a complicated function of electron energy, reflecting the

energy loss and scattering of the initial electrons during transport through the bulk material. Such spectra are the subject of photoelectron spectroscopy and are a powerful tool in surface analysis. However, the electron energy distribution is also an important element in modeling detector time response.

As shown in Fig. 2, the spectrum is primarily a two component system consisting of the photo and Auger electrons and a secondary electron spectrum peaked at a few eV with a few eV half-width. With this type of spectrum, a simple retarding-potential spectrometer(18) can be used to measure the relative primary and secondary contributions.

In this measurement, a reverse bias is applied to the photocathode and only electrons above a critical voltage can escape and contribute to the "high energy yield," $Y_{H.E.}$. Subtracting the photocathode quantum efficiencies measured under forward and reverse bias conditions produces the "low energy yield," $Y_{L.E.}$. The ratio of the low to high energy electron yield for gold in the 1 to 10 keV photon energy range is shown in Fig. 7 as reprinted from Gaines, et al.(19) This level of information is sufficient for modeling photodiode time response.

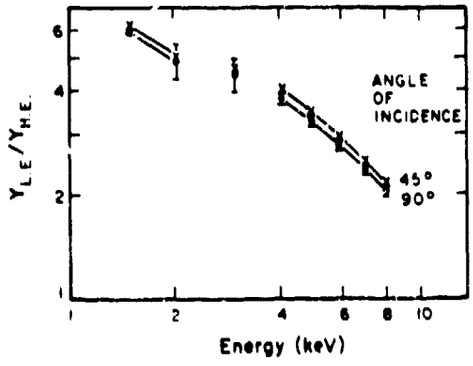

Fig. 7. The ratio of low energy (<5 eV) electron yield, $Y_{L.E.}$, to high energy (>10 eV) electron yield, $Y_{H.E.}$, for a .104 mg/cm² gold foil.(19)

For other applications, such as predicting streak camera time response at the few picosecond level, more detailed secondary electron energy distribution information is required. Such studies have been undertaken by Henke, et al.(14) using an electrostatic focusing electron spectrometer. A sample of the data for Au excited by Al K x-rays is reprinted in Fig. 8. The solid lines shown in this figure are fits to Henke's semiemperical model of photoyield and demonstrate that the shape predictions are acceptable.

However, this model predicts an absolute yield which is a factor of three too small for the case shown here. This occurs because the model only handles secondary electron scattering empirically. The assumption is made that the secondary electron distribution shape is only slightly modified by secondary electron scattering while the absolute numbers of secondaries is increased.

This model has been extended to insulators and semiconductors(15) where the presence of a band gap restricts the phase-space for electron scattering. The case of insulators is particularly interesting because small energy loss electron-phonon scattering and/or density of states distributions generate structures in the secondary electron energy distribution. A guide to these and additional electron distribution measurements is contained in Table II of the Appendix.

C. Angular Distributions, $d^2N/d\Omega d\phi$

The electron emission process is dependent upon both the photon angle of incidence relative to the cathode surface, θ, and on the angle, ϕ, at which the electrons are emitted relative to the cathode surface. These distributions are important since angle of incidence is frequently used to reduce the incident x-ray flux by going to grazing angle or to enhance electron emission(20).

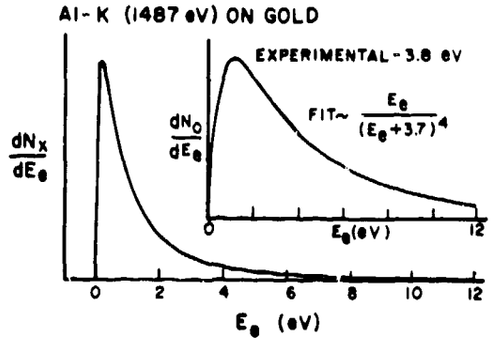

Fig. 8. Secondary electron distribution from gold at 105°C in a 3 x 10^{-8} Torr vacuum. The lower curve is the distribution as measured by the spectrograph of Henke(14) and the upper curve has been corrected for the instrument response and is the electron distribution at the photocathode surface. The solid line is a fit to Henke's semiempirical model.

The standard technique for measuring quantum efficiency vs photon incidence angle is reported by Gaines and Hansen(19). In this experiment, a simple parameter such as total yield or primary to secondary electron ratio is monitored as a function of photon angle of incidence. For angles greater than a few degrees, quantum efficiency decreases as 1/sinθ due to decreased photon deposition within a secondary electron escape depth as reported by both Gaines and Hansen(20) and by Ganeev and Izrailev(21).

An enhanced "no loss" primary photoelectron yield is seen for photon incidence angles just above the critical angle for total x-ray reflection(20). This effect is due to increased photon deposition within a primary photoelectron escape depth of the cathode surface when the photons are refracted nearly parallel to the photocathode surface. This effect will decrease the time response of a photodiode detector due to a decrease in the electron flight time across the anode-cathode spacing.

The more complicated measurement of electron emission versus ϕ is much less commonly reported. Henke's model of secondary yield predicts a Lambertian, sinθ, dependence to the secondary emission resulting from isotropy of the secondary distribution below the photocathode surface. This assumption, however, is not valid for all primary electrons and data from Fernstein and Smith(18) and Baird and Fadley(22) contain such results.

Angular distribution photoemission data is summarized in Table III of the Appendix. It is compiled by element and angle of incidence or emission.

D. Enhanced Photoemission

Studies of total yield(23-26) and secondary electron distribution(14) have indicated that certain alkali halides, iodides, and semiconductors exhibit enhanced secondary electron emission under x-ray excitation. A comparison of CsI data with Au is shown in Fig. 9. Over most of the energy range from 1 to 10 keV, CsI shows an enhanced photoemission by a factor of

30. This allows significant latitude in designing systems with greater low flux sensitivity.

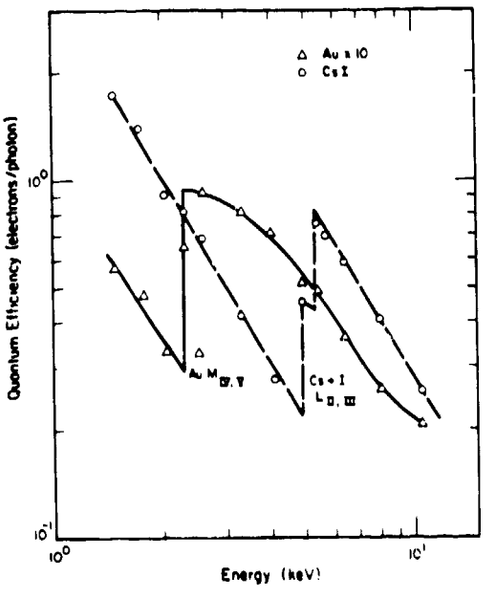

Fig. 9. A comparison of quantum efficiency for gold and cesium iodide photocathodes.

This effect for dielectrics can be understood qualitatively by noting the increased scattering length for low energy electrons below the fermi level. This allows electrons to be collected from deeper within the cathode resulting in higher electron yield.

This enhancement does not come without penalty, however. First, the alkali iodides are deliquescent and care must be taken to maintain them in a water-vapor free environment. We know that heat sealing CsI photocathodes in plastic bags filled with dry nitrogen and storing them in a dessicator will induce no apparent degradation in cathode appearance for as long as six months. However, exposure of these cathodes to air at 20 to 25% relative humidity for more than a few hours impairs performance.

Second, the time response of these cathodes may be less rapid. The emission process seems to have a slower component at the level of a few percent of the main emission which persists for approximately 100 picoseconds(27). Furthermore, effects caused by large photoemissive currents and the finite cathode material resistivity may cause time dependent sensitivity. At present, these materials show promise as useful photoemissive cathodes but care should be taken to carefully characterize their energy and time response until further study answers some of these outstanding concerns.

Another class of enhanced photoemissive materials based upon gallium-arsenide and gallium-arsenic-phosphide has been reported by Bardas et al.(28). These materials show quantum efficiencies of 100 at 2 keV x-ray energy. Of even greater interest, is the linear increase of quantum efficiency with x-ray energy. However, these materials are very sensitive to vacuum contaminants and are generally used at less than 10^{-10} torr. This greatly limits their practical application.

PHOTOCATHODE AGING EFFECTS

Aging effects similar to those seen on alkali iodide cathodes are also present on any metallic surface. Photoelectric emission is a surface physics effect and any change in the surface composition or structure will appear as a change in the secondary electron yield. Some discussion of long term aging is available in the literature(25,29), but historically, most photocathodes have been utilized in sealed vacuum environments where aging effects are minimal.

Experience at the Los Alamos National Laboratory, LANL, indicates that with care, photocathodes can be used for extended periods of time in the laser fusion experimental environment as subkilovolt, x-ray transducers without large, >15%, changes in system calibration. Photocathode surface preparation is important to achieve this level of stability. Figure 10 is a long term aging study of micromachined aluminum cathodes. It shows that for this type of surface quantum efficiency changes of less than 10% are possible over six months exposure to air. These cathodes are used in the LANL low energy x-ray spectrometer at the HELIOS laser facility. They are used behind replaceable filter windows and are exposed to the laser chamber vacuum on each shot. Between shots, the diodes are housed in a selfcontained ion pumped vacuum system. Several aging and use studies at LANL indicate that an absolute calibration of better than ±15% can be maintained over four months in the operational environment.

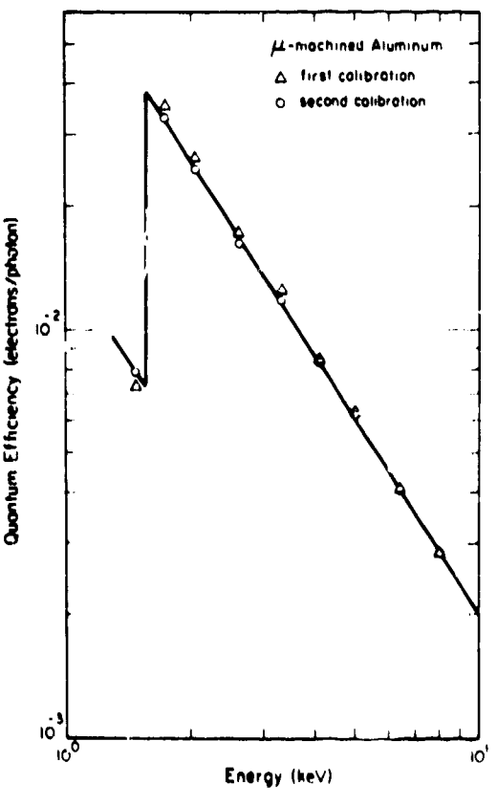

Fig. 10. A before and after comparison of cathode quantum efficiency for micromachined aluminum. The two calibrations are separated by six months storage in air.

Less stringent manufacturing and handling precautions can have a very damaging effect on absolute photocathode sensitivity as shown in Fig. 11. This before and after comparison is described in detail by Day, et al.(25) and includes a one month use on the LANL GEMINI laser facility during which time the

cathodes were conintually exposed to the target chamber vacuum.

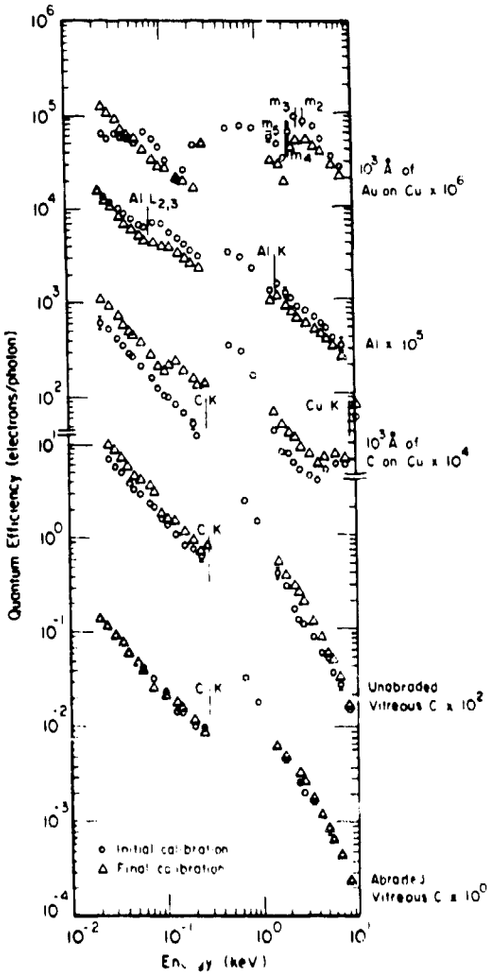

Fig. 11. The quantum efficiency of gold, aluminum, carbon, and abraded and unabraded vitreous carbon. The cathodes were stored in air for six months and used in the LANL GEMINI laser facility between calibrations.

The aging effects for these samples can exceed plus or minus a factor of two. Obviously, significant care must be taken in handling photocathodes for windowless detector applications. The procedure we have adopted to use windowless detectors(25) is to establish a reproducible photocathode manufacturing process and to replace and recalibrate photocathodes frequently, every few weeks.

APPLICATIONS

The primary purpose of this paper has been to discuss the status of photoelectric emission measurements as they apply to subkilovolt x-ray diagnostics. The topic of this section will be the practical application of photoemission measurements in an absolutely calibrated time resolved x-ray spectrometer for laser fusion plasma diagnostics.

The detectors are simple biplanar x-ray sensitivity photodiodes, XRD's, in a seven element array covering the spectral range from 20 eV to 2 keV with low resolving power, $\varepsilon/\Delta E \approx 1$-9. The detector system's acronym is MULTIFLEX for multiple fast low energy x-ray detector. XRD's are simple detectors consisting of an x-ray cathode and anode mesh. The photoelectric current resulting from x-rays impinging on the photo-

The energy dependent response of the system is determined by the energy dependent sensitivity of the photocathode convolved with the filter window transmission. The sensitivity of four typical channels is shown in Fig. 12.

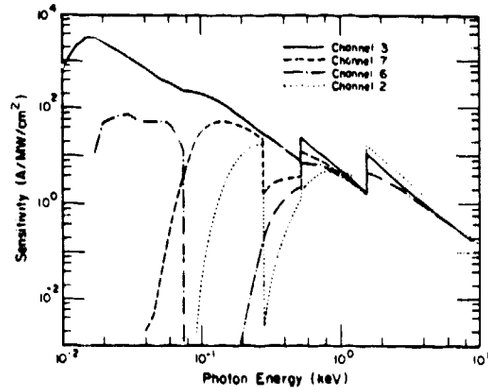

Fig. 12. Typical MULTIFLEX response functions.
Channel 3 - bare photocathode plus three layers of Ni mesh.
Channel 7 - 70 μg/cm² of polypropylene plus three layers of Ni mesh.
Channel 6 - 7600 Å of Aluminum plus three layers of Ni mesh.
Channel 2 - 272 μg/cm² Kimfoil pluss 400 Å of aluminum.

The risetime of the detector is determined by the photoelectron flight time across the anode-cathode gap; while the decay-time is given by the decay-time of the anode-cathode gap capacitance into the characteristic impedance of the signal line. The detectors we have built for MULTIFLEX have a full-width-at-half-maximum, FWHM, time response of 75 ps; which is more than adequate to measure the 1 ns x-ray pulses from CO_2 laser plasmas.

The data consists of seven oscilloscope traces showing detector currents versus time, all common timed to ±50 ps. These currents are sampled at 100 ps time intervals and used as inputs to a deconvolution code. This code accepts the absolutely calibrated detector response curves, the set of seven detector currents, and iteratively minimizes the difference between the most recent spectrum and the observed currents. A typical time resolved spectra for a glass microballoon irradiated by 8.2 TW of CO_2 laser light is shown in Fig. 13.

SUMMARY

The MULTIFLEX system is one of several detectors we will hear about in this conference, which utilizes photoelectric emission in the detection of soft x-radiation. Photoelectric emission is a complicated spatial, energy, angular, and temporally dependent process and our empirical and theoretical understanding is not sufficient to model all potential device performance criteria.

In this paper, the most important parameters which are used to describe photoemission have been discussed and it was indicated how they affect detector system performance. An outline of the measurement techniques has been provided and typical data was shown in comparison with available models. The Appendix provides a guide to the literature where the interested reader can go for data and details of the measurements. Photoemission studies have played a vital role in the development of modern physics and the detailed study of this process will continue to be important in our pulsed plasma diagnostic instrumentation.

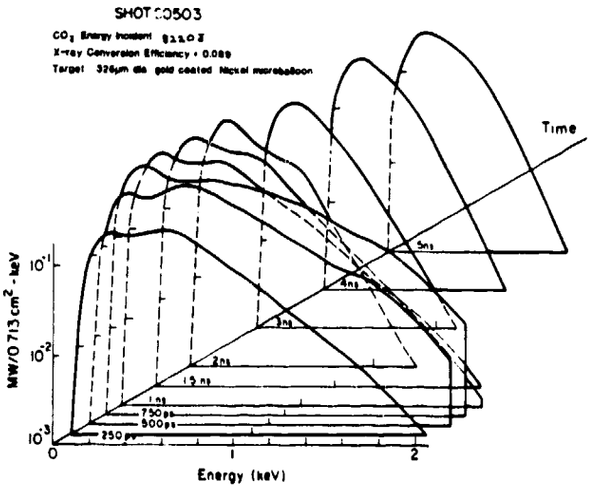

Fig. 13. Time resolved x-ray spectra from a gold coated nickel microballoon irradiated with 8.2 TW of 10.6 μm CO_2 laser light.

ACKNOWLEDGEMENTS

I would like to thank Dr. Burton Henke for many useful discussions on this subject and J. Gaines for permission to use his experimental results. I would especially like to thank Robert Hockaday for much hard work in assembling, checking, and collating the data in the Appendix.

REFERENCES

1. H. Hertz, "Uber Einen Finflug des Ultravioletten Lichtes auf die Electrische Entladung," Wiedemannsche Annalen der Physik, 31, pp. 982-1000 (1887).
2. A. Schuster, "Experiments on the Discharge of Electricity Through Gases," Proceedings of the Royal Society of London (A), 42, pp. 371-379 (1887).
3. S. Arrhenius, "Uber das Leitungsvermögen der Phosphorescirenden Luft," Wiedemannsche Annalen der Physik, 32, pp. 545-572 (1887).
4. A. Einstein, "Uber Einen die Erzeugung und Verivandlung des Lichtes Betreffenden Heuristischen Gesichtspunkt," Annalen der Physik, 17, pp. 132-148 (1905).
5. R. A. Millikan, "A Direct Photoelectric Determination of Plank's 'h'," Physical Review, 7, pp. 355-388 (1916).
6. A. H. Compton, "The Spectrum of Secondary Rays," Physical Review, 19, pp. 267-268 (1922).
7. R. H. Pratt, A. Ron, and H. K. Tseng, "Atomic Photoelectric Effect Above 10 keV," Rev. Mod. Phys., 45, p. 273 (1973).
8. B. L. Henke and F. S. Ebisu, "Low Energy X-Ray and Electron Absorption Within Solids," Adv. in X-ray Anal., 17, pp. 150-213 (1973).
9. W. J. Viegele, E. Briggs, L. Bates, E. M. Henry, and R. Bracewell, "X-Ray Cross Section Compilation from 0.1 keV to 1 MeV," Kaman Sciences Corporation Report KN-71-431(R) (1971).
10. E. Storm and H. I. Israel, "Photon Cross Sections from 1 keV to 100 MeV for Elements Z = 1 to Z= 100," Nuc. Data Tables, 7, p. 565 (1970).
11. W. H. McMaster, N. K. Del Grande, J. H. Mallett, and J. H. Hubbell, "Compilation of X-Ray Cross Sections," Lawrence Livermore Report UCRL 50174 (1969).
12. H. J. Hagemann, W. Gudat, and C. Kunz, "Optical Constants from the Far Infared to the X-Ray Region: Mg, Al, Cu, Au, Pi, C, and Al_2O_3," Deutches Flektronen-Synchrotron Report, DESY SR-74/7 (1974).
13. J. H. Weaver, C. Krafka, D. W. Lynch, and F. F. Koch, "Optical Properties of Metals I: The Transition Metals, 0.1 ≤ hν ≤ 500 eV Ti, V, Cr, Mn, Fe, Co, Ni, Zr, Nb, Mo, Ru, Ph, Pd, Hf, Ta, W, Re, Os, Ir, Pt," Deutches Flektronen - Synchrotron Report, DESY F41 (1981).
14. B. L. Henke, J. A. Smith, and David T. Attwood, "0.1-10-keV X-Ray-Induced Electron Emissions from Solids - Models and Secondary Electron Measurements," J. App. Phys., 48, pp. 1852-1866 (1977).
15. B. L. Henke, J. Liesegang, and S. D. Smith, "Soft X-Ray-Induced Secondary-Electron Emission from Semiconductors and Insulators: Models and Measurements," Phys. Rev. B., 19, p. 3004 (1979).
16. G. Beck, "Photodiode and Holder with 60-psec Response Time," Rev. Sci. Instrum., 47, p. 849 (1976).
17. R. H. Day, P. Lee, E. B. Saloman, and D. J. Nagel, "X-Ray Diodes for Laser Fusion Plasma Diagnostics," Los Alamos Report, LA-7941-MS (1981).
18. M. J. Bernstein and J. A. Smith, "Primary and Secondary Photoelectron Yields Induced by Soft X-Rays," IEEE Trans. on Nuc. Sci., 26, pp. 4978-4983 (1979).
19. J. L. Gaines and B. A. Hansen, "Ultrasoft-X-Ray Reflection, Refraction and Production of Photoelectrons (100-1000-eV Region)," J. Appl. Phys., 47, pp. 3923-3928 (1976).
20. B. L. Henke, "X-Ray-Induced Electron Emission from Thin Gold Foils," Phys. Rev. A, 6, p. 94 (1972).
21. A. S. Ganeev and I. M. Izrailev, "Photoelectric Yield for Soft X-Rays," Sov. Phys. - Tech. Phys. 31, p. 270 (1961).
22. R. J. Baird and C. S. Fadley, "X-Ray Photoelectron Angular Distributions with Dispersion-Compensating X-ray and Electron Optics," J. of Elec. Spec. and Rel. Phenom., 11, pp. 39-65 (1977).
23. L. G. Eliseenko, V. N. Shchemelev, and M. A. Rumsh, "Quantum Yields of the Surface X-Ray Photoeffect at 1-10Å," Sov. Phys. - Tech. Phys., (English Translation) 13, pp. 122-129 (1968).
24. E. P. Saloman, J. S. Pearlman, and B. L. Henke, "Evaluation of High Efficiency CsI and CuI Photocathodes for Soft X-Ray Diagnostics," Appl. Opt., 19, pp. 749-753 (1980).
25. R. H. Day, P. Lee, E. P. Saloman, and D. J. Nagel, "Photoelectric Quantum Efficiencies and Filter Window Absorption Coefficients from 20 eV to 10 keV," to be published in J. of Appl. Phys.
26. B. L. Henke, J. P. Knauer, and K. Premaratne, "The Characterization of X-Ray Photocathodes in the 0.1-10 keV Photon Energy Region," J. of Appl. Phys. 52, pp. 1509-1520 (1981).
27. G. L. Stradling, H. Medecki, R. L. Kauffman, D. T. Attwood, and B. L. Henke, "Relative Responses of CsI and Au Photocathodes to 70-psec, 500-eV X-Ray Pulses," Appl. Phys. Lett., 37, pp. 782-784.
28. D. Pardee, E. Kellogg, and S. Murray, "Detection of Soft X-Rays with NEA III-V Photocathodes," Rev. Sci. Instr., 49, pp. 1273-1278 (1978).
29. R. P. Cairns and J. A. R. Samson, "Metal Photocathodes as Secondary Standards for Absolute Intensity Measurements in the Vacuum Ultraviolet," J. Opt. Soc. Am., 56, pp. 1568-1573 (1966).

APPENDIX

The Appendix consists of four major components: 1) a master list of most references on photoemission data above 10 eV in aphabetical order by author; 2) a table of availalbe quantum efficiency data listed by element or compound and incident photon energy; 3) a table of electron energy distribution data by element and 4) a table of electron and photon angular distribution data by element and angle of incidence or emission.

In the tables the reference numbers refer to the master reference list. In Tables I and II, the numbers in parenthesis following the reference number refer to the exciting photon energy in eV unless the photon energy is marked in other units. In Table I, a "P" following the reference number indicates a measurement of primary photoelectron quantum efficiency, and in Table II, an asterisk, " " preceding a reference number indicates an unusual broad-band x-ray source. In Table III, the numbers in parenthesis are angles in degress.

Reference List

1. L. Apker, E. Taft, and J. Dickey, "Electron Scattering and the Photoemission from Cesium Antimonide," J. Opt. Soc. Am. 43, p. 78, (1952).
2. R. F. Baker, "A Grating Monochromater for the Schumann Region," J. Opt. Soc. Am. 28, p. 55 (1938).
3. R. J. Baird and C. S. Fadley, "X-Ray Photoelectron Angular Distributions With Dispersion-Compensating X-Ray and Electron Optics," J. Elec. Spect. Rel. Phen. 11, p. 39, (1977).
4. D. Baradas, E. Kellogg, S. Murray, and R. Enck, Jr., "Detection of Soft X Rays with NEA III-V Photocathodes," Rev. Sci. Instr. 49, p. 1773, (1978).
5. J. E. Bateman and R. J. Apsimon, "A New Photocathode for X-Ray Image Intensifiers Operating in The 1-50 keV Region," Adv. Elec. Phys. 52, p. 189 (1979).
6. M. J. Bernstein, "Photoelectron Energy Spectra Generated by Low-Energy X-Rays From Intense Plasmas," IEEE Trans. Nuc. Sci. 24, p. 2512, (1977).
7. M. J. Bernstein and J. A. Smith, "Primary and Secondary Photoelection Yields Induced by Soft X-Rays," IEEE Trans. Nuc. Sci. 26, p. 4078, (1979).
8. M. J. Bernstein and K. W. Paschen, "Forward and Backward Photoemission Yields From Metals at Various X-Ray Angles of Incidence," IEEE Trans. Nuc. Sci. 20, p. 6, 111, (1973).
9. M. A. Blokhin, E. G. Orlova, I. G. Shveitzer, and G. Kokh, "Ultrasoft X-Ray Spectra of Inorganic Compounds of Beryllium," Seriya Fizicheskaya, 40, p. 91, (1976).
10. J. N. Bradford "X-Ray Induced Electron Emission II," IEEE Trans. Nuc. Sci. 20, 5, p. 105, (1973).
11. E. J. T. Burns and J. F. Thurston, "The Use of Some Metal Photocathodes for Absolute Intensity Measurements in the Soft X-Ray-Vacuum Ultraviolet," Appl. Spec. 31, p. 317, (1977).
12. R. B. Cairns and J. A. R. Samson, "Metal Photocathodes as Secondary Standards for Absolute Intensity Measurements in the Vacuum Ultraviolet," J. Opt. Soc. Am. 56, p. 1568, (1966).
13. L. R. Canfield, R. G. Johnston, and R. P. Madden, "NBS Detector Standards for the Far Ultraviolet," Applied Optics 12, p. 1611, (1973).
14. R. H. Day and F. J. T. Burns, "Absolute Calibration of Photoelectric Diodes," Advances in X-Ray Analysis, 19, p. 597, (1976).
15. R. H. Day, P. Lee, E. B. Saloman, and D. J. Nagel, "X-Ray Diodes for Laser Fusion Plasma Diagnostics," IEEE International Conf. on Plasma Sci. (Invited Paper), LA-UR-79-1360 or LA-7941-MS, June 1979.
16. J. Dickey, "New Aspects of the Photoelectric Emission from Na and K," Phys. Rev. 81, p. 612, (1951).
17. T. H. DiStefano and W. E. Spicer, "Photoemission from CsI: Experiment," Phys. Rev. B, 7, p. 1554, (1973).
18. S. W. Duckett and P. H. Metzger, "Intrinsic Photoemission of Alkali Halides," Phys. Rev. 137, A953, (1965).
19. L. Dunkelman, "Ultraviolet Photodetectors," J. Quant. Spectrosc. Radiat. Transfer, 2, p. 533, (1962).
20. P. J. Ebert, J. L. Gaines, and G. R. Leipelt, "Measurement of X-Ray-Induced Electron Currents from Metal Targets," Lawrence Livermore Laboratory Report No. UCRL-50691, (1969).
21. L. G. Eliseenko, V. N. Shchemelev, and M. A. Rumsh, "Quantum Yields of the Surface X-Ray Photoeffect at 1-10 A," Sov. Phys.-Tech. Phys. 13, p. 122, (1968).
22. J. G. Endriz and W. E. Spicer, "Experimental Evidence for the Surface Photoelectric Effect in Aluminum," Phys. Rev. Lett. 27, p. 570, (1971).
23. D. A. Fromme, V. A. J. Van Lint, R. Strettner, and C. Mallon, "Electron Emission Spectra Produced by Exploding-Wire Photon Sources," IEEE Trans. Nuc. Sci. 24, p. 2527 (1977).
24. J. L. Gaines and R. A. Hansen, "X-Ray-Induced Electron Emission from Thin Gold Foils," J. Applied Phys. 47, p. 3923, (1976).
25. A. S. Ganeev and I. M. Ignatiev, "Photoelectric Yield for Soft X-Rays," Sov. Phys. - Tech. Phys. 31, p. 270, (1961).
26. G. W. Goetze, A. H. Boerio, and M. Green, "Field-Enhanced Secondary Electron Emission From Films of Low Density," J. Appl. Phys. 35, p. 482 (1963).
27. F. Görlich, "Über zusammengesetzte, durchsichtige Photokathoden," Z. Phys. 101, p. 335 (1936).
28. M. Ya Grudskii, A. V. Klyshenkov, and V. V. Smirnov, "Electron Yield From Metals Under the Action of 30 to 90 keV Photon Radiation," Sov. Phys.-Tech. Phys. 21, p. 172, (1976).
29. H. J. Hagemann, W. Gudat, and C. Kunz, "Optical Constants From the Far Infared to the X-Ray Region: Mg, Al, Cu, Ag, Pt, C, and Al_2O_3," DESY-report SR-74/7, May 1974.
30. W. J. Harper and W. J. Choyke, "Semitransparent Photocathodes at Low Temperatures," Rev. Sci. Instr. 27, p. 966, (1956).
31. P. L. Hartman, "Investigations on Some Alkali Halides in the Vacuum Ultraviolet," J. Quant. Spectrosc. Radiat. Transfer, 2, p. 579, (1962).
32. B. L. Henke, "The Characterization of Photocathodes for Application to Time-Resolved X-Ray Spectroscopy," Technical Progress Report (April, 1979), DOE Cont. No. DE-AS03-76SF00235.
33. B. L. Henke, "Some Recent Studies in Low Energy X-Ray Physics," in lab review.
34. B. L. Henke, "Ultrasoft-X-Ray Reflection Refraction and Production of Photoelectrons (100-1000 eV Region)," Phys. Rev. A 6, p. 94, (1972).
35. B. L. Henke, J. A. Smith, and D. T. Attwood, "0.1-10 keV X-Ray-Induced Electron Emission From Solids - Models and Secondary Electron Measurements," J. Appl. Phys 48, p. 1852, (1977).
36. B. L. Henke, J. A. Smith, and D. T. Attwood, "Secondary Electron Energy Distribution for Gold as Excited by C K (277 eV) and Al K (1487 eV) X Rays," Appl. Phys. Lett. 29, p. 539, 1976.
37. B. L. Henke, "On the Theory and Development of X-Ray Photocathode Systems for Applications in High Temperature Plasma Diagnostics," Progress Report, April, 15, 1977.
38. B. L. Henke, "Models and Measurement for the Response of Dielectric X-Ray Photocathodes," Tech. Report, March 1978 (in lab).

39. B. L. Henke, X-Ray Spectroscopy in the 100-1000 eV Region," Nuc. Instr. Meth. 177, p. 161 (1980).
40. B. L. Henke, J. Liesegang, and S. D. Smith, "Soft X-Ray-Induced Secondary-Electron Emission From Semiconductors and Insulators: Models and Measurements," Phys. Rev. B, 19, p. 3004 (1979).
41. B. L. Henke, J. P. Knauer, and K. Premaratne, "The Characterization of X-Ray Photocathodes in the .1-10 keV Photon Energy Region," Bull. Am. Phys. Soc. 24, p. 1098 (1979).
42. H. E. Hinteregger, "Photoelectric Emission in the Extreme Ultraviolet," Phys. Rev. 96, p. 538 (1954).
43. H. E. Hinteregger and K. Watanabe, "Photoelectric Cells for the Vacuum Ultraviolet," J. Opt. Soc. Am. 43, p. 604, (1953).
44. C. S. Inouye and W. Pong, "Ultraviolet Photoelectron Spectra for Rubidium Halides," Phys. Rev. B., 15, p. 2265, (1977).
45. I. M. Izrailev, "Photoelectric Yield for Soft X-Rays," Sov. Phys.-Technical Phys. 7, p. 1020, (1963).
46. C. Kenty, "Photoelectric Yields in the Extreme Ultraviolet," Phys. Rev. 44, p. 891, (1933).
47. Zh. Kh. Khachatryan, A. E. Melamid, and A. A. Guzhov, "Study of Photoelectric Emission in the Vacuum Ultraviolet," Bulletin of the Academy of Sciences, USSR Physical Series 35, p. 574, (1971).
48. G. S. Kvater and E. D. Mischenko, "Multielectron Nature of Cesium-Antimony Photocathode Photoemission in the Ultraviolet," Optics & Spectrosc. (Eng. Trans.) 33, p. 57, (1971).
49. A. P. Lukirskii, E. P. Savinov, I. A. Brytov, and Yu. F. Shepelev, "Efficiency of Secondary-Electron Multipliers with Au, LiF, MgF_2, SrF_2, BeO, KCl, and CsI, Photocathodes in the 23.6 to 113 Å Wavelength Region," Bull. Acad. Sci., USSR Phys. Ser. 28, p. 774, (1964).
50. A. P. Lukirskii, M. A. Rumsh, and I. A. Karpovich, "Measurement of the Photoelectric Yield of the External Photoeffect Under the Action of X-Rays in the Wavelength Range 1.54-13.3Å," Optics and Spectroscopy 9, p. 343, (1960).
51. A. P. Lukirskii, M. A. Rumsh, and L. A. Smirnov, "Measurement of the Photoelectric Yield for Ultrasoft X-Radiation," Optics and Spectroscopy 9, p. 265, (1960). (Optika i spektro)
52. F. H. Metzger, "On the Quantum Efficiencies of Twenty Alkali Halides in the 12-21 eV Region," J. Phys. Chem. Solids, 26, p. 1879, (1965).
53. C. Mori and T. Watanabe, "Photoelectric Emission of Metals by X-Rays in the keV Region," Japanese J. Appl. Phys. 9, p. 666, (1970)
54. N. G. Nakhodkin and P. V. Melnik, "A Comparative Study of the Energy Distribution of Secondary Electrons and Photoelectrons Excited by Soft X-Rays," Soviet Phys.-Solid State 10, p. 1462, (1968).
55. Yu. A. Nemilov and V. E. Privalova, "On the Influence of Alkali Metals Upon the Properties of Antimony Photocathodes," Sov. Phys-Solid State, 2, p. 1189, (1960).
56. H. Petersen and S. B. M. Hagstrom, "Optical Excitation of teh Surface Photoelectric Effect of Metals Using Synchotron Radiation," Phys. Rev. Lett. 41, p. 1314, (1978).
57. W. Pong, "Photoemission from Al-Al_2O_3 Films in the Vacuum Ultraviolet Region," J. Appl. Phys., 40, p. 1733, (1969).
58. W. Pong and C. S. Inouye, "Ultraviolet Photoemission Study of LiF," J. Elec. Spec. Rel. Phenomena 11, p. 165, (1977).
59. W. Pong and J. A. Smith, "Photoemission Studies of LiCl, NaCl, and KCl," Phys. Rev. B, 9, p. 2674 (1974).
60. W. Pong, R. Sumida, G. Moore, "Attenuation Length for Photoelectrons in Metal Films," J. Appl. Phys. 41, p. 1869 (1969).
61. H. C. Rentschler, D. E. Henry, and K. O. Smith, "Photoelectric Emission From Different Metals," Rev. Sci. Instr. 3, p.794 (1932).
62. M. A. Rumsh and V. N. Shchemelev, "Role of Secondary Emission Phenomena in the X-Ray Photoeffect in Metallic Cathodes," Soviet Physics - Solid State 5, p. 46, (1963).
63. E. B. Saloman, "Typical Photoefficiency Between 20-250 eV of Windowless XUV Photodiodes With Tungsten and Anodized Aluminum Oxide Photocathodes," Applied Physics, 17, p. 1489, (1978).
64. E. B. Saloman and D. L. Ederer, "Absolute Radiometric Calibration of Detectors Between 200-600 A," Applied Optics, 14, p. 1029, (1975).
65. E. B. Saloman, J. S. Pearlman, and B. L. Henke, "Evaluation of High Efficiency CsI and CuI Photocathodes for Soft X-Ray Diagnostics," Applied Optics, 19, p. 749, (1980).
66. J. A. R. Samson, "Absolute Intensity Measurements in the Vacuum Ultraviolet," J. Opt. Soc. Am. 54, p. 6, (1964).
67. J. A. R. Samson and R. B. Cairns, "Photoelectric Yield of Aluminum From 300 to 1300 A," Rev. Sci. Instr. 36, p. 19, (1965).
68. F. P. Savinov and A. P. Lukirskii, "The Efficiency of Secondary Electron Multipliers With Au, Al, Ni, LiF, MgF_2, SrF_2, CsI, KCl, and BeO Photocathodes at Wavelengths of 75-300 A," Optika i Spectrosk (USSR) (English trans. - Optics and Spectrosc.) 23, p. 163, (1967).
69. F. P. Savinov, A. P. Lukirskii, and Yu. F. Shepelev, "The Problem of External Photoeffect of Metal Photocathodes for Radiation of Wavelength 23.6-113 A," Sov. Phys. - Solid State 6, p. 2624 (1965).
70. V. N. Shchemlev, L. P. Eliseenko, E. P. Denisov, and M. A. Rumsh, "Current and Pulse Measurements of the X-Ray Photoemission of a Massive Cathode," Soviet Physics - Solid State 6, p. 2051, (1965).
71. V. N. Schemelev and M. A. Rumsh, "X-Ray Photoeffect in Dielectric Cathodes," Sov. Phys. - Solid State 5, p. 43, (1963).
72. Yu. A. Shuba and I. V. Smirnova, "Photoemission of Electrons by Copper and Silver Iodides," Soviet Phys. - Solid State 6, p. 1201, (1960). (Fizika Tverdogo Tela)
73. W. E. Spicer, "Photoemissive, Photoconductive, and Optical Absorption Studies of Alkali-Antimony Compounds," Phys. Rev. 112, p. 114, (1958).
74. W. E. Spicer and R. L. Bell, "The III-V Photocathode: A Major Detector Development," Pub. Astron. Soc. Pacific 84, p. 110, (1972).
75. D. J. Strickland, "Soft X-Ray Photoemission," IEEE Trans. Nuc. Sci. 24, 2499, (1977).
76. J. L. Stanford, R. N. Hamm, and E. T. Arakawa, "Effect of Photon Refraction on Angular Dependence of Photoelectric Yields in the Wavelength Region 300-1200 A," J. Opt. Soc. Am. 56, p. 124, (1966).
77. A. Suna and R. H. Tait, "Ultraviolet Photon Induced Secondary Electron Emission from TiO_2: Theory and Experiment," Solid State Comm. 29, p. 215, (1979).
78. E. A. Taft and H. R. Philipp, "Photoelectric Emission From the Valence Band of Some Alkali Halides," J. Phys. Chem. Solids 3, p. 1, (1957).
79. E. Taft and L. Apker, "Photoemission From Cesium and Rubidium Tellurides," J. Opt. Soc. Am. 43, p. 81, (1953).
80. L. Van Speybroeck, E. Kellogg, S. Murray, and S. Duckett, "Negative Affinity X-Ray Photocathodes," IEEE Trans. Nuc. Sci. 21, p. 408, (1974).
81. N. Wainfan, W. C. Walker, and G. L. Weissler, "Preliminary Results on Photoelectric Yields of Pt and Ta and on Photoionization in O_2 and N_2 in the Vacuum Ultraviolet," J. Appl. Phys. 24, p. 1318, (1953).

82. W. C. Walker and G. L. Weissler, "Excitation of the Sodium D Lines in the Nightglow," Phys. Rev. 97, p. 1178, (1954).
83. W. C. Walker and G. L. Weissler, "Vacuum Ultraviolet Optical and Photoelectric Effects in Solids," J. Quant. Spectrosc. Radiat. Transfer 2, 613, (1962).
84. W. C. Walker, N. Wainfan, and G. L. Weissler, "Photoelectric Yields in the Vacuum Ultraviolet," J. Appl. Phys. 26, p. 1366, (1955).
85. W. C. Walker, O. P. Rustgi, and G. L. Weissler, "Optical and Photoelectric Properties of Thin Metallic Films in the Vacuum Ultraviolet," J. Opt. Soc. Am. 49, p. 471, (1959).
86. J. H. Weaver, C. Krafka, D. W. Lynch, and E. E. Koch, "Optical Properties of Metals I: The Transition Metals, 0.1 ≤ hν ≤ 500 eV," DESY F 41, HASYLAB 81/01, Jan. 1981.

Table I

Quantum Efficiencies

Acetone	19(8-12)
AQUADAG	23(1.2-3.3 keV)
Arrodag	7(1-6 keV), 7P(1-6 keV)
Ag	85(6-30), 12(10-62), 84(12-25), 61(4-5), 28(30-90 keV), 45(.5-30 keV), 23P(1.2-3.3 keV), 25(4-6 keV), 7(1-6 keV), 7P(1-6 keV), 28P(30-90 keV), 20(6-100 keV)
AgCl	31(6-10), 38(1487)
AgI	72(5-11), 31(6-10)
Al	83(7-27), 85(7-27), 12(9-62), 14(0.01-10 keV), 32(100-1000), 21(1200-8000), 53P(1.7-8 keV), 65(21-248), 75(0.1-10 keV), 15(0.01-10 keV), 11(0.01-1.5 keV), 61(4-5), 28(30-90 keV), 70(8000), 22(6-12), 45(4-30 keV), 62(8000), 12(10-62), 68(41-124), 60(7-12), 23P(1.2-3.3 keV), 25(4-6 keV), 7(1-6 keV), 7P(1-6 keV), 28P(3080 keV), 70P(8000), 62P(8000), 67(10-41), 20(10-60 keV), 69(109, 185, 284, 304, 525)
Al-Mg	12(12-31)
Al$_2$O$_3$	57(8-21), 64(10-65), 63(20-250), 28P(30-75 keV), 7(1-6 keV), 7P(1-6 keV), 32(100-1000) 66(14-31)
Au	85(8-27) 12(10-62), 24(1.5-8 keV), 21(1200-8000), 49(109-525), 53P(1.7-8 keV), 65(21-245), 66(10-31), 84(12-25), 15(0.01-10 keV), 39(100-1000), 76(10-41), 28(30-90 keV), 70(8000), 62(8000), 68(41-124), 60(7-12), 23P(1.2-3.3), 30 (.5-8 keV), 30P(.5-8 keV), 7(1-7 keV), 7P(1-7 keV), 32(100-1000), 28P(30-90 keV), 70P(8000), 62P(8000), 13(21), 20(10-100 keV), 41(0.1-1 keV), 41P(0.1-10 keV)
B	61(2-4)
BaF	61(2-4)
Be	42(8-17), 12(10-62), 51(100-500)
BeO	10(4-12), 49(109-525), 72(3.5-11), 9(110-140), 68(41-124)
BeCl$_2$	9(110-140)
Be(OH)$_2$	9(110-140)
BeSO$_4$·4H$_2$O	9(110-140)
Be$_3$(PO$_4$)$_2$	9(110-140)
Bi	85(8-27), 70(8000), 62(8000), 70P(8000), 62P(8000)
C	15(0.01-10 keV), 23P(1.2-3.3 keV)
CS$_2$	19(8-12)
Ce	61(4-5)
CaF$_2$	21(1200-8000), 51(100-500), 71(8000), 71P(8000)
Ce	61(3-5)

Cd	85(8-27), 2(4-12), 61(4-5)
CdS	74(7-25)
Co	45(8000), 67(8000), 70P(8000), 62P(8000)
CONSTANTAN	46(10-20)
CORTEX-O GLASS	61(3-5)
Cr	15(0.01-10 keV), 70(8000), 45(5-30 keV), 62(8000), 62P(8000), 70P(8000)
CsBi	30(2-3.5), 27(1.5-3)
CsBr	19(5-12), 78(7-11), 52(12-22)
Cs-C, O-Ag	27(1.3-3.0)
CsCl	21(1200-9000), 78(7-11), 52(12-22), 70(8000), 70P(8000)
CsF	52(12-22)
CsI	19(5-12), 17(5-12), 32(100-1000), 21(1200-9000), 46(100-750), 50(1-8 keV), 78(7-11), 52(12-22), 65(21-248), 5(0-60 keV), 15(1-10 keV), 39(100-1000), 39(25-310), 72(3.5-13), 31(6-11), 70(8000), 68(41-124), 65(21-248), 70P(8000), 78(6-11), 52(12-22), 41(0.1-10 keV), 41P(0.1-10 keV)
(Cs)NaK,Sb	73(1.3-4.3)
Cs,Sb	1(1-6), 74(2-1, (1.6-4)
Cs-Bi	27(1.6-3)
Cs-C, O-Ag	27(1.4-3)
Cs-Sb	19(4-12), 30(2-3.5), 27(1.5-3.0)
CsTe	19(3.5-6), 30(2-3.5)
Cs,Te	70(3.4-6)
Cu	21(1200-8000), 8m(6-31), 11(0.1-1.5 keV), 61(4-5), 28(30-90 keV), 46(5-30 keV), 62(8000), 62P(8000), 28P(30-90 keV), 12(12-31), 17(4-11), 12(12-21), 17(4-11), 15(0.1-10 keV
Cu-CsI	46(4-11
CuI	19(4-12), 47(7-25), 65(1-248), 78(4-11), 41(0.1-10 keV), 41P(0.1-10 keV)
CuAlMg-Pt	7(3.2-5)
ETHELENE OXIDE	19(8-12)
ETHYL SULFIDE	19(8-12)
Fe	12(10-82), 11(0.1-1 keV), 70(8000), 70P(8000),
GaAs-Cs	74(2-12)
GaAs-(Cs),	8(0.5-4 keV)
GaAS	47(7-25), 74(1-12)
GLASS	7(1-6 keV), 78(1-6 keV)
Ir	8(8-27), 12(10-82)
InAsP	74(1-12)
K	10(2-6), 27(1.5-3.0)
K_2HeF_4	9(110-140)
KBr	19(5-12), 18(8-22), 78(8-11), 52(12-22), 70(8000), 21(1200-9000), 70P(8000)
KCl	18(8-22), 21(1200-9000), 46(100-750), 78(8-11), 31(8-12, 52(12-22), 70(8000), 71(8-30), 68(41-124), 70P(8000), 71P(8000), 20(5-9 keV)

KF	18(8-22), 78(10.5-11), 52(12-22)
KI	18(8-22), 21(1200-9000), 78(2-12), 31(7-11), 52(12-22)
KSt	55(2-6)
K_2St	73(1.8-4.6)
Kr	66(14-31)
LiBr	18(8-22), 52(12-22)
LiCl	18(8-22), 52(12-22)
LiF	18(8-22), 21(1200-9000), 51(100-500), 49(109-750), 58(10-24), 31(7-17), 52(12-22), 68(41-124)
LiI	18(8-22), 78(6-10), 52(12-22)
LiSt	55(2-6)
Mg	46(10-20), 61(3-5)
MgF_2	13(10-2[illegible]), 49(109-750), 71(8000), 68(41-124), 71B(8000)
MgO	72(5.5-13)
Mo	12(10-62), 45(.5-30 keV), 84(9-25)
MYLAR	7(1-6 keV), 78(1-6 keV)
N_2	[illegible]
Na	[illegible]
NaBr	18(8-22), [illegible] keV), 52(12-22)
NaCl	18(8-22), [illegible]
Na_3AlF_6	[illegible]
NaF	[illegible], 52(12-22)
NaI	18(8-22), [illegible]
[illegible]	[illegible]
[illegible]	[illegible]
[illegible]	[illegible]
[illegible]	[illegible]
[illegible]	[illegible]
[illegible]	[illegible]
Ne	[illegible]
Ni	[illegible] keV), [illegible]
O_2	84(12-2[illegible])
[illegible]	[illegible]
[illegible]	[illegible]
Pd	84(12-2[illegible])
Pt	[illegible], 50(1-8 keV), [illegible]
[illegible]	[illegible]
RbBr	52(12-22)
RbCl	21(1200-9000), 52(12-22)

RbF	52(12-22)
RbI	19(5-12), 78(7-11), 52(12-22)
RbSb	30(2-3.5)
RbTe	19(4-8), 30(2-3.5)
Rb_3Sb	73(1.6-4)
$RbI(NaK_2)Sb$	73(1.4-3.5)
Sc	15(0.01-10 keV)
SARAN	7(1-6 keV), 7P(1-6 keV)
Si	47(7-25), 7(1-6 keV), 7P(1-6 keV)
Sn	83(7.5-27), 85(8-27), 12(10-62), 21(1200-8000), 70(8000), 70P(8000), 62(8000), 62P(8000), 20(10-100 keV)
SrF_2	19(4-12), 21(1200-9000), 51(100-500), 49(109-750), 50(1-8 keV), 68(41-124), 72(3.25-13)
Ta	19(4-6), 12(10-62), 81(12-25), 61(4-8), 45(.5-30 keV), 12(10-62), 25(4-8 keV), 20(10-100 keV)
Te	21(1200-8000), 79(1.5-6), 62(8000), 62P(8000)
Ti	12(10-62), 21(1200-8000), [illegible](1-8 keV), 11(0.1-1.5 keV), 61(4-8), 70(8000), 7(1-6 keV), 7P(1-6 keV), 70P(8000), [illegible] keV)
Tl	61(3-8)
W	[illegible]
[illegible]	[illegible]
[illegible]	[illegible]
Xe	[illegible]
Zn	[illegible]
Zr	[illegible]

Table II

<u>Electron Energy Distribution</u>

Ar	[illegible] keV
Al	[illegible]
Al_2O_3	[illegible] keV)
AgCl	[illegible]
Au	[illegible]
C	[illegible] keV)
[illegible]	[illegible] keV)
CsI	[illegible]

CsI	17(4.5–10.2), 40(1486), 65(277), 39(277, 8048), 38(1487), 37(1487), 65(277), 32(1487), 47(7.1, 7.88, 10.2, 11.6, 13.3, 18.6), 41(277, 800)
CsINaKSb	48(2, 8.5)
Cs_2Te	79(6.7, 6.19, 5.38, 4.89)
Cs–Sb	48(2.1, 8.5)
Cu	10(14–50 keV)
CuI	40(1487), 65(277), 39(277, 8048), 38(1487), 37(1487), 65(277), 32(1487), 41(277, 8000)
GaAsP	4(.85, 1.25, 1.49, 2.17, 2.98 keV)
Ge	40(1487), 82(10, 18), 54(1.5, 4.5, 8 keV), 32(1487)
K	16(3.39, 3.96, 4.89, 6.71)
KBr	40(1487), 38(1487)
KCl	40(1487), 59(12–19), 36(1487), 37(1487)
KI	40(1487), 38(1487), 37(1487)
Kr	66(15)
LiCl	40(1487), 59(17–23)
LiF	82(13–27), 38(1487), 40(1487)
Mg	71(5[illegible]
P	1[illegible] keV
Na I	[illegible]
NaI	[illegible]
Ne	[illegible]
Ni	[illegible]
Ni	[illegible]
NiO	[illegible]
Ni	[illegible]
NiO	[illegible]
Ni	[illegible]
O	[illegible]
OsO$_4$	[illegible]
Pb	[illegible] keV, [illegible] keV
Pd	[illegible]
Rb	[illegible]
Se	[illegible]
Si	[illegible]
SiO$_2$	[illegible]
Sn	[illegible]
SnO$_2$	[illegible]
Ta	[illegible]
Te	[illegible]

Table III

Angular Distribution

Ag	25(15°, 35°, 45°, 60°)
Al	67(0°-90°), 68(0°-40°), 69(0°-40°), 25(15°, 35°, 45°, 60°), P(0°-80°)
Au	24(30°, 45°, 60°, 75°, 90°), 68(0°-40°), 34(0°-6°), 6(0°, 60°, 90°, 180°), 75(0°, 45°, 70°), 20(30°, 60°, 90°)
BeO	49(0°-40°)
C	3(1°, 10°, 20°, 30°, 40°, 50°, 60°, 70°, 80°, 90°, 95°)
CsI	49(0°-40°), 68(0°-40°)
Cu	8(0°-80°)
KCl	49(0°-40°), 68(0°-40°)
LiF	49(0°-40°), 68(0°-40°)
MgF$_2$	13(0°-75°), 49(0°-40°), 68(0°-40°)
Pt	7(0°, 45°, 70°)
SrF$_2$	49(0°-40°), 68(0°-40°)
Ta	25(15°-60°), 10(0°-70°), P(0°-80°)
Ti	8(0°-90°)
W	25(15°-60°)